Spike patterning of a stochastic phase model neuron given periodic inhibition

William H. Nesse,[1] Gregory A. Clark,[2] and Paul C. Bressloff[1]
[1]*Department of Mathematics, University of Utah, Salt Lake City, Utah 84112, USA*
[2]*Department of Bioengineering, University of Utah, Salt Lake City, Utah 84112, USA*
(Received 27 November 2006; published 26 March 2007)

We present a phase model of a repetitively firing neuron possessing a phase-dependent stochastic response to periodic inhibition. We analyze the dynamics in terms of a stochastic phase map and determine the invariant phase distribution. We use the latter to compute both the distribution of interspike intervals (ISIs) and the stochastic winding number (mean firing rate) as a function of the input frequency. We show that only low-order phase locking persists in the presence of weak phase dependence, and is characterized statistically by a multimodal ISI distribution and a nonmonotonic variation in the stochastic winding number as a function of input frequency.

DOI: 10.1103/PhysRevE.75.031912 PACS number(s): 87.19.La, 87.19.Nn, 05.40.−a

I. INTRODUCTION

A major question in the study of nervous system function is how information is encoded in the spike trains of repetitively firing neurons. One common experimental paradigm for investigating the relationship between input and output spike trains is a pacemaker neuron undergoing periodic inhibitory stimulation [1–4]. A key observation is that a neural oscillator exhibits phase-locking regimes, where increasing through a range of inhibitory input frequencies can paradoxically elevate the neuron's firing rate. If the frequency is pushed past this range then the phase locking breaks down, resulting in phase drift and a decreased firing rate. Theoretical studies have demonstrated that similar behavior occurs in a variety of nonlinear oscillator models [5–7]. It has also been found experimentally that the nonmonotonic relationship between input and output firing rates due to phase locking can be disrupted by introducing random fluctuations in the input spike trains, resulting in monotonic behavior [1,4]. The response of a pacemaker cell to noisy pulse trains has recently been analyzed in terms of a stochastic phase map, with the distribution of phases evolving according to a linear Frobenius-Perron (FP) operator [8]. One of the useful features of such an operator is that its spectral properties can be used to define and analyze stochastic phase locking and stochastic bifurcations [9,10].

In this paper we study the effects of intrinsic rather than input noise on the response of a pacemaker neuron to a periodic inhibitory spike train. We model the neuron as a phase oscillator with a noisy phase resetting curve (PRC), whose dynamics reduce to a stochastic phase map. This formulation is motivated by experimentally derived PRCs that have been found to be noisy [11,12]. From the stochastic phase map we determine the invariant phase distribution of the associated FP operator, and use this to compute both the distribution of interspike intervals (ISIs) and the stochastic winding number (mean firing rate) as a function of the input frequency. These calculations allow us to investigate how phase locking vanishes as the noise level is increased. We find that phase-locking regions with long periods, where many cycles of stimuli are required to complete the phase patterning, tend to be destroyed by small amounts of noise. On the other hand, low order phase locking persists up to a critical level of noise, and is characterized statistically by a multimodal ISI distribution and a nonmonotonic variation in the stochastic winding number as a function of input frequency. In related work it has been shown how fluctuations in phase resetting curves can also have nontrivial effects on the synchronization properties of a pair of pulse-coupled neural phase oscillators [13]. In particular, a noise-induced bifurcation can switch the pair from a synchronous to an antisynchronous state. Beyond the models dealt with here, noise can have important constructive effects on neuronal oscillator systems such as noise induced synchronization of chaotic oscillations and synchronization of uncoupled ensembles of oscillators by a common noisy input [14,15].

II. THE PHASE MODEL

Consider a repetitively spiking neuron as defined by the phase variable on the circle $\theta_A \in [0,1)$ where we arbitrarily define the spike event to occur when θ_A crosses 1 from below. In the absence of inputs, θ_A cycles at a constant frequency ω_A. Inputs are generated by another oscillator θ_B with frequency ω_B. Whenever neuron A receives a pulselike input, its phase is shifted by a phase-dependent quantity known as its phase resetting curve (PRC). That is, $\theta_A \to \theta_A + R(\theta_A) + S(\theta_A)\xi$, where $R(\theta)$ is the deterministic part of the PRC and $S(\theta)\xi$ is a phase-dependent random contribution. The random variable ξ has probability density $Q(\xi)$ and the multiplier $S(\theta) > 0$ is the phase-dependent modifier of the variance of ξ. This system can be written as the discontinuous differential equation

$$\dot{\theta}_A = \omega_A + [R(\theta_A) + S(\theta_A)\xi(t)]\delta(\theta_B),$$

$$\dot{\theta}_B = \omega_B = 1/T_B, \tag{1}$$

where $\delta(\theta)$ is the dirac delta function and we will set $\omega_A = 1$ for simplicity. Without the noise term this type of model has been studied for many years in the context of circle maps [16]. The model can be understood phenomenologically, or

in the case of sufficiently weak inputs, can be derived from more complex multidimensional conductance-based models using phase-reduction methods [17,18]. In order to simplify our subsequent analysis, we impose two conditions on the phase shift induced by an input spike. First, an input spike cannot cause the phase to jump forward across unity so that the neuron fires. This is reasonable, because we are assuming that the input is inhibitory. Second, an input cannot retard the phase to such an extent that on the next input spike the phase is behind where it was on the previous input. That is, we preclude oscillator death in the model. Hence we require

$$P[-T_B < \theta + R(\theta) + S(\theta)\xi < 1] = 1, \quad \forall\ \theta_A \in [0,1). \tag{2}$$

Notice that we allow the phase to pass backward through zero. If an oscillator is slowed so it passes back through zero and then subsequently advances forward through zero then we could confusingly count this as a spike, and doing so would produce nonphysiological spike statistics. In the present analysis we distinguish between this case and advancement through unity to spike.

The model equation (1) is solved by generating a mapping of phases for the time of the nth input pulse to the $(n+1)$th. Let ϕ_n be the phase of neuron A immediately before the nth input. Immediately after the input the phase is $\phi_n + R(\phi_n) + S(\phi_n)\xi_n$ and the phase of A just before the $(n+1)$th input is

$$\phi_{n+1} = T_B + \phi_n + R(\phi_n) + S(\phi_n)\xi_n = f(\phi_n, \xi_n), \tag{3}$$

where ξ_n are independent, identically distributed random variables. Consider $\phi \in \mathbb{R}$ and let $p_n(\phi)$ be a density of phases of A just before the nth input. The $(n+1)$th density is found to be [13]

$$p_{n+1}(\phi) = \int_{\mathbb{R}} Q\left(\frac{\phi - \phi' - T_B - R(\phi')}{S(\phi')}\right)\frac{p_n(\phi')}{S(\phi')}d\phi'$$
$$= F(p_n)(\phi). \tag{4}$$

We would like to view these phases modulo one by identifying $\phi \in [0,1)$ with $\phi + j$ for $j \in \mathbb{Z}$ so we define $q_n(\psi) = \Sigma_{j\in\mathbb{Z}} p_n(\psi + j)$ for $\psi \in [0,1)$. Hence the operator in Eq. (4) is transformed to the "modulo one" FP operator

$$q_{n+1}(\psi) = \int_0^1 \sum_{j\in\mathbb{Z}} Q\left(\frac{\psi - \psi' + j - T_B - R(\psi')}{S(\psi')}\right)\frac{q_n(\psi')}{S(\psi')}d\psi'$$
$$= G(q_n)(\psi). \tag{5}$$

FP theory can guarantee the existence of a limiting density q^* from iterates $G^n(q_0) = G(q_{n-1}) = q_n$ that is invariant with respect to G: $G(q^*) = q^*$ [19]. The invariant density q^* gives the steady-state distribution of phases. To compute q^* in practice we discretize the integral operator (5) into a matrix. The invariant density vector q^* is the eigenvector with a single dominant unit eigenvalue.

A. Calculation of relative spike time distribution

We wish to use q^* to derive the distribution of impulse times τ. That is, given neuron A has just fired, when will the next input spike arrive? We denote the corresponding probability density by $p_{AB}(\tau)$, where the subscripts signify that τ is the relative time from the A spike to the next B input. We sketch the construction of $p_{AB}(\tau)$ as follows. We consider a population of oscillators each of which receives an input spike at time $t=0$, say, with the distribution of phases just prior to the input given by the invariant density q^*. We then chart the evolution of the population by keeping track of when each neuron first fires and determining the time from this event to the arrival of the next input spike. We proceed iteratively by decomposing the probability distribution of relative times τ according to how many input spikes a neuron receives before it fires [see Fig. 1(b)]. If the stimulation frequency is larger than the natural frequency ($T_B < 1$), then none of the oscillators will fire twice before receiving an input, thus reducing the complexity.

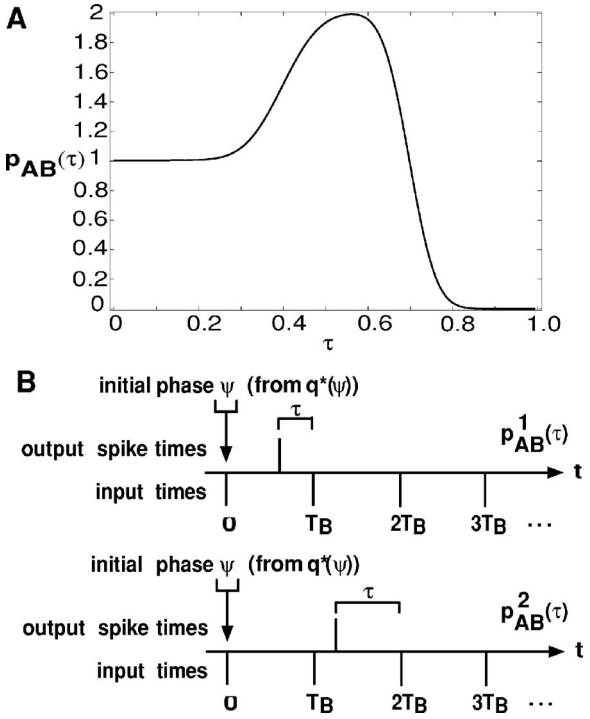

FIG. 1. (a) $p_{AB}(\tau)$ for the equations $\phi_{n+1} = T_B + \phi_n + a_0 + z$ with $z \sim N(0,\sigma)$, $a_0 = -0.2$, $\sigma = 0.05$, and $T_B = 0.9$. Notice that even with $R(\theta) = a_0$ (no phase-dependent coupling) the distribution of relative timings still has a single mode of more likely input times. (b) Schematic diagram showing the construction of $p_{AB}(\tau)$ from the terms $p^j_{AB}(\tau)$: The initial phase ψ at time $t=0$ occurs with probability $q^*(\psi)d\psi$. Some of these phase trajectories, comprising the density $G_1(q^*)(\tau) = p^1_{AB}(\tau)$, spike at time $T_B - \tau$ before the next input at $t = T_B$ [top row of panel (b)]. Others starting at the initial phase ψ spike after $t = T_B$ but before $t = 2T_B$. These phase trajectories comprise the density $G_1[G_0(q^*)](\tau) = p^2_{AB}(\tau)$, shown in the bottom row of panel (b). Phase trajectories that spike in the time interval $[2T_B, 3T_B)$ (not shown) comprise the density $G_1\{G_0[G_0(q^*)]\}(\tau) = p^3_{AB}(\tau)$, etc.

To formalize the calculation, it is useful to decompose the operator G of Eq. (5) as $G = \Sigma_{j\in\mathbb{Z}} G_j$ with

$$G_j(q_n)(\psi) = \int_0^1 Q\left(\frac{\psi - \psi' + j - T_B - R(\psi')}{S(\psi')}\right) \times \frac{q_n(\psi')}{S(\psi')} d\psi'. \quad (6)$$

Here $G_j(q_n)$ determines the component of the probability density q_{n+1} arising from neurons that fire j times between one input spike and the next. Additionally, because we have scaled $\omega_A = 1$, the phase ψ represents the time τ between firing and the subsequent input. Hence, by decomposing G into the sum of G_j, we can obtain relative timing information. We also note that the lower bound in Eq. (2) implies that $G_j = 0$ for $j < 0$. Hence, $G = \Sigma_{j \geq 0} G_j$. Starting with the invariant density q^* we define

$$p^1_{AB}(\tau) = G_1(q^*)(\tau). \quad (7)$$

This represents the population of oscillators that fire a time τ prior to the arrival of the first input spike at $t = T_B$ (assuming that the previous input occurred at time $t = 0$). The density $G(q^*) = \Sigma_{j \geq 2} G_j(q^*)$ represents the population of oscillators that have fired twice or more before the subsequent input occurs. For stimulation frequencies greater than the intrinsic frequency of neuron A this density is zero: $\Sigma_{j \geq 2} G_j(q^*) = 0$. Next we map $G_0(q^*)$, which represents the population of oscillators that have not yet fired after one cycle of inputs, to $G_1[G_0(q^*)]$ and define

$$p^2_{AB}(\tau) = G_1[G_0(q^*)](\tau). \quad (8)$$

This is the probability density of oscillators that have fired a time τ prior to the arrival of the second input spike at $t = 2T_B$. Similarly, the density $G_0^{(2)}(q^*)(\psi) = G_0 G_0(q^*)(\psi)$ corresponds to the remaining oscillators that after two cycles of inputs have not fired. From this we define, in general,

$$p^k_{AB}(\tau) = G_1[G_0^{(k-1)}(q^*)](\tau) \quad (9)$$

to be the relative timing density of the spike to the next (kth) input after $k-1$ preceding input cycles. Summing $p^k_{AB}(\tau)$ we arrive at the density of relative timings

$$p_{AB}(\tau) = \sum_{j=1}^{\infty} p^j_{AB}(\tau), \quad \tau \in [0, \min\{T_B, 1\}). \quad (10)$$

An example of $p_{AB}(\tau)$ is shown in Fig. 1(a). In the case $T_B > 1$, for which $\Sigma_{j \geq 2} G_j(q^*) > 0$, there are some oscillators that do not receive an input between successive output spikes. This means that $\int_0^1 p_{AB}(\tau) d\tau < 1$ and the proportion of oscillators that do not receive an input is $1 - \int_0^1 p_{AB}(\tau) d\tau$.

B. Calculation of interspike interval distribution

We can compute the ISI distribution by first computing the conditional ISI density given the relative input time τ. We denote this by $p_{AA}(T|\tau)$, where the subscripts indicate that T is the time between successive output spikes of neuron A. The conditional density can be decomposed according to how many input spikes occur between successive output spikes. First, suppose $\tau < T < T_B + \tau$, that is, the neuron receives only a single input spike between successive firing events. Let ψ denote the phase of the neuron when the next input spike arrives (see Fig. 2). It follows that $T = T_B + \tau - \psi$ with ψ related to τ according to $1 + \psi = f(\tau, \xi)$ and f defined in Eq. (3). This produces the conditional ISI density

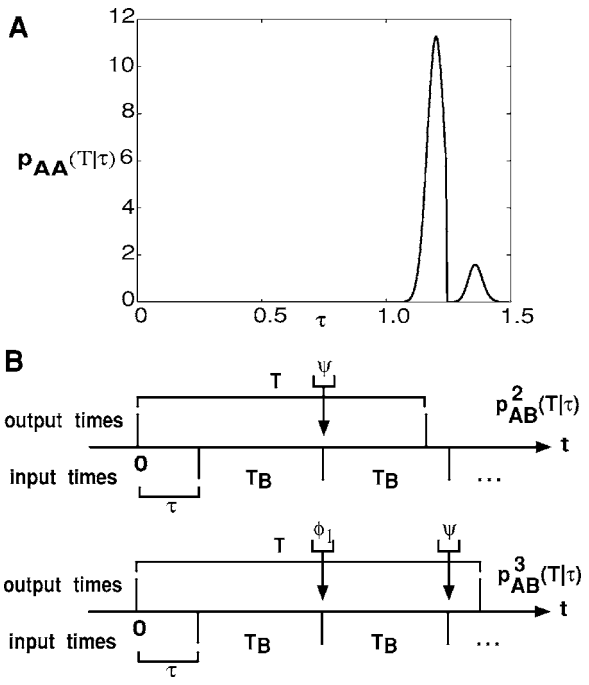

FIG. 2. (a) $p_{AA}(T|\tau)$ for the equations $\phi_{n+1} = T_B + \phi_n + a_0 + \xi$ with $\xi \sim N(0, \sigma)$, $a_0 = -0.1$, $\sigma = 0.025$, $\tau = 0.25$, and $T_B = 0.5$ ($\omega_B = 2$). The discontinuities occur at $T = kT_B + \tau$, $k = 1, 2, \ldots$, and reflect the separation of oscillators that fire after k inputs. (b) Below the graph is an idealized representation of likely spike trains (output times) in response to inputs (input times), given the first input was at $\tau = 0.25$. For this particular case the most likely interspike intervals are found in the intervals $[2T_B + \tau, 3T_B + \tau)$ and $[3T_B + \tau, 4T_B + \tau)$, associated with the respective probability densities $p^2_{AA}(T|\tau)$ and $p^3_{AA}(T|\tau)$.

$$p^1_{AA}(T|\tau) = Q\left(\frac{T - 1 + R(\tau)}{S(\tau)}\right)\frac{1}{S(\tau)}. \quad (11)$$

We are assuming that $Q(\xi)$ is an even function of ξ. Now suppose that the neuron receives two inputs before firing again so that $T \in [T_B + \tau, 2T_B + \tau)$. Let ϕ_1 be the phase of the neuron when the second input spike arrives and let ψ denote the phase when the third spike arrives [see Fig. 2(b)]. Then $T = 2T_B + \tau - \psi$ with $1 + \psi = f(\phi_1, \xi')$ and $\phi_1 = f(\tau, \xi)$ for independent random variables ξ, ξ'. It follows that the conditional ISI density for $T \in [T_B + \tau, 2T_B + \tau)$ is

$$p^2_{AA}(T|\tau) = \int_{T_B}^{\infty} Q\left(\frac{T - \tau - t' + R[\phi_1(t' + \tau)]}{S[\phi_1(t' + \tau)]}\right) \times \frac{1}{S[\phi_1(t' + \tau)]} p^1_{AA}(t' + \tau|\tau) dt', \quad (12)$$

where we have introduced the change of variables $\phi_1(t) = 1 - (t - \tau) + T_B$. Similarly, if $T \in [(j-1)T_B + \tau, jT_B + \tau)$, $j = 1, 2, \ldots$, then the corresponding conditional ISI density is

$$p_{AA}^{j}(T|\tau) = \int_{(j-1)T_B}^{\infty} Q\left(\frac{T-\tau-t'+R[\phi_{(j-1)}(t'+\tau)]}{S[\phi_{(j-1)}(t'+\tau)]}\right) \times \frac{1}{S[\phi_{(j-1)}(t'+\tau)]} p_{AA}^{(j-1)}(t'+\tau|\tau)dt', \quad (13)$$

with $\phi_j(t)=1-(t-\tau)+jT_B$. We therefore obtain the full conditional ISI density

$$p_{AA}(T|\tau) = p_{AA}^{j}(T|\tau), \quad T \in [(j-1)T_B+\tau, jT_B+\tau). \quad (14)$$

$p_{AA}(T|\tau)$ is defined for $T\in[0,\infty)$ and $\lim_{T\to\infty} p_{AA}(T|\tau)=0$. Recall that the lower bound of Eq. (2) requires that all oscillators cannot be phase retarded over an input cycle T_B, guaranteeing that all oscillators eventually reach unity. Consequently, the computation of $p_{AA}(T|\tau)$ can be accomplished in finitely many recursive integrals $p_{AA}^{j}(T|\tau)$. $p_{AA}(T|\tau)$ will have discontinuities at the boundaries of the intervals $jT_B+\tau$, $j=1,2,\ldots$ [see Fig. 2(a)]. These discontinuities are the boundaries between populations of cycles that were fast enough to be able to reach firing threshold before another input ($T<jT_B+\tau$) and those which were too slow ($T\geq jT_B+\tau$).

In the above analysis we have assumed that an input spike cannot immediately drive a neuron to fire. This will be valid provided that the upper bound of Eq. (2) holds. However, it is possible for a neuron to fire twice without receiving an input. In that case, the ISI is simply the natural frequency of the oscillator, $T=1$. Taking this into account, the density of interspike intervals $p_{AA}(T)$ can be calculated by integrating the product of Eqs. (14) and (10) with respect to τ giving the final result

$$p_{AA}(T) = \int_0^1 p_{AA}(T|\tau)p_{AB}(\tau)d\tau + \delta(T-1)\left(1-\int_0^1 p_{AB}(\tau)d\tau\right). \quad (15)$$

In performing the numerical computations required for $p_{AA}(T)$ one may wonder if it is computationally efficient compared with performing Monte Carlo simulations. At first sight, the series of nested integrals needed to compute the $p_{AA}^{j}(T|\tau)$ would seem to be prohibitively expensive because each integral, when reduced to a discrete mesh, transforms to matrix multiplication. We must also compute the dominant eigenvector q^* of the FP operator G as well as transforming q^* to approximate $p_{AB}(\tau)$, all of which takes many matrix multiplications. Although initially daunting, with the appropriate choice of a discrete mesh the analytical calculations can be made efficient. Let N be the number of grid points evenly spaced on the interval $[0,1)$ with step size $1/N$ between points. We shall also choose the same step size for T and τ, and require that T_B be a multiple of $1/N$. With these conditions the integral kernel in Eq. (13) can be constructed once and reused to compute all $p_{AA}^{j}(T|\tau)$. We expect the analytical method to be fast when there are few nested integrals $p_{AA}^{j}(T|\tau)$ to compute and slower when there are many. There will be many when the phase delay magnitude $|R(\theta)|$ nears the length of T_B. In this case the delay is so big that only a very small phase advance is made over a stimulation cycle and we are nearing the lower bound in constraint (2). For model parameters that avoid this pitfall the analytical computations can be done efficiently and can be performed faster, more accurately, and have the advantage of being analyzable, than Monte Carlo simulations (data not shown).

III. STATISTICAL PHASE LOCKING, AVERAGE FIRING RATE, AND SPIKE PATTERNING FOR AN INHIBITORY INPUT

We now use the probability densities derived in the preceding section to analyze the effects of noise on the response of a pacemaker neuron to periodic inhibition.

A. Phase locking and stochastic winding number

In the deterministic case ($\xi=0$), 1:1 phase locking occurs when there is a fixed point ψ^* of the circle map (3), $\psi^*-1=f(\psi^*,0)$. Likewise, $n:m$ phase locking occurs when $\psi^*-m=f^n(\psi^*,0)$, where f^n is the nth iterate of f. The qualitative dynamics of the deterministic circle map can be characterized in terms of its winding number [20]

$$\Omega_A = \lim_{n\to\infty}\frac{\phi_n}{n}, \quad (16)$$

which measures the mean firing rate per number of inputs of the neuron. Assuming that the map f is smooth and invertible, it can be shown that Ω_A is independent of the initial phase ϕ_0 and is a continuous function of parameters. If Ω_A is rational, that is, $\Omega_A=m/n$ for integers m,n, then every sequence of phases converges to a periodic orbit on which there is $n:m$ phase locking. On the other hand, if Ω_A is irrational then the dynamics is quasiperiodic with the sequence of phases ϕ_n dense on the interval $[0,1)$. The winding number as a function of T_B exhibits a devil's staircase structure in which neighborhoods centered about $T_B=m/n$ (in which $\int_0^1 R=0$) can be shown to be constant, equaling m/n, representing $n:m$ phase-locked regions. The compliment set of the $n:m$ phase-locked regions forms a cantor-set structure [20]. Because Ω_A is continuous in T_B it guarantees that $\Omega_A(T_B)$ is monotonically increasing. In the present context we wish to dimensionalize the winding number to make it synonymous with mean firing rate per input time cycle by scaling the winding number by T_B. Scaling by T_B makes the devil's staircase structure slanted and the phase-locked regions become monotonically decreasing segments. If we switch to the $\omega_B=1/T_B$ line the segments become monotonically increasing and we refer to them as paradoxical regions. One of the main points of this document is to show how the inclusion of noise can flatten and obscure these paradoxical segments.

If there exists noise in the system then we can calculate the stochastic winding number, scaled by T_B, following Ref. [8]. Let the initial phase of an oscillator just before an input be θ. The phase ϕ just before the next stimulus is distributed according to the density

$$Q\left(\frac{\phi-\theta-T_B-R(\theta)}{S(\theta)}\right)\frac{1}{S(\theta)}. \tag{17}$$

The mean phase traveled in the time between the two inputs is

$$w(\theta)=\int_{-\infty}^{\infty}(\phi-\theta)Q\left(\frac{\phi-\theta-T_B-R(\theta)}{S(\theta)}\right)\frac{1}{S(\theta)}d\phi$$
$$=T_B+R(\theta), \tag{18}$$

assuming that the noise density $Q(\xi)$ has zero mean. The stochastic winding number is then

$$\Omega_{A,\text{stoch}}=\frac{1}{T_B}\int_0^1 w(\theta)q^*(\theta)d\theta$$
$$=1+\frac{1}{T_B}\int_0^1 R(\theta)q^*(\theta)d\theta. \tag{19}$$

B. Perturbation expansion of stochastic winding number

For concreteness, suppose that $R(x)=a_0+\epsilon r(x)$, $a_0<0$, and $S(x)=1+\epsilon s(x)$ with $0\le\epsilon\ll 1$. When $\epsilon=0$ there is no robust phase locking and the stochastic winding number is simply

$$\Omega_{A,\text{stoch}}=1+\frac{a_0}{T_B}=1+a_0\omega_B. \tag{20}$$

Hence, in the absence of phase locking, the firing rate decreases linearly in ω_B. With $\epsilon>0$ we require a perturbative solution to q^*. It is convenient to work with the periodic extension of q^*, which we denote by p^*. The latter is invariant with respect to the linear operator F of Eq. (4). Let

$$p^*(\phi)=p_0^*(\phi)+\epsilon p_1^*(\phi)+\epsilon^2 p_2^*(\phi)+\cdots \tag{21}$$

and expand the operator F in powers of ϵ. Collecting terms with equal powers of ϵ generates a hierarchy of equations. The zeroth order equation is

$$p_0^*(\phi)=\int_{-\infty}^{\infty}p_0^*(x)Q(\phi-x-\Theta)dx, \tag{22}$$

where $\Theta=T_B+a_0$, which has the solution $p_0^*(\phi)=1$. The first order equation takes the form

$$p_1^*(\phi)-\int_{-\infty}^{\infty}Q(\phi-x-\Theta)p_1^*(x)dx$$
$$=-\int_{-\infty}^{\infty}Q(\phi-x-\Theta)s(\phi)dx-\int_{-\infty}^{\infty}Q'(\phi-x-\Theta)[r(x)$$
$$+(\phi-x-\Theta)s(x)]dx. \tag{23}$$

Rearranging and using the change of variables $z=\phi-x-\Theta$ and integration by parts produces the inhomogeneous linear integral equation

$$p_1^*(\phi)-\int_{-\infty}^{\infty}Q(z)p_1^*(\phi-z-\Theta)dz$$
$$=-\int_{-\infty}^{\infty}zQ(z)s'(\phi-z-\Theta)dz-\int_{-\infty}^{\infty}Q(z)r'(\phi-z-\Theta)dz. \tag{24}$$

The solution of the integral equation can be solved by Fourier methods. We let

$$r(x)=\sum_n a_n\cos(2\pi nx)+b_n\sin(2\pi nx),$$

$$s(x)=\sum_n c_n\cos(2\pi nx)+d_n\sin(2\pi nx),$$

$$p_1^*(x)=\sum_n \alpha_n\cos(2\pi nx)+\beta_n\sin(2\pi nx) \tag{25}$$

and then note that if Q is Gaussian, $Q(x)=(\pi\sigma^2)^{-1/2}\exp(-x^2/\sigma^2)$, then

$$u_n=\int_{-\infty}^{\infty}Q(x)\cos(2\pi nx)dx=\exp[-(n\pi\sigma)^2],$$

$$v_n=\int_{-\infty}^{\infty}xQ(x)\sin(2\pi nx)dx=\pi\sigma^2 nu_n. \tag{26}$$

A Gaussian random variable violates the restriction in Eq. (2). However, if σ is small enough the violations will be rare events and inconsequential to the results. Substituting Eq. (25) into Eq. (24) and then matching terms we arrive at the following 2×2 linear system for the nth Fourier coefficients:

$$\frac{1}{2\pi n}\begin{pmatrix}1-u_n\cos(2\pi n\Theta) & u_n\sin(2\pi n\Theta)\\ -u_n\sin(2\pi n\Theta) & 1-u_n\cos(2\pi n\Theta)\end{pmatrix}\begin{pmatrix}\alpha_n\\ \beta_n\end{pmatrix}$$
$$=-\begin{pmatrix}U_n\cos(2\pi n\Theta)+V_n\sin(2\pi n\Theta)\\ -V_n\cos(2\pi n\Theta)+U_n\sin(2\pi n\Theta)\end{pmatrix}, \tag{27}$$

where $U_n=v_nc_n+b_nu_n$ and $V_n=d_nv_n+a_nu_n$. The matrix is always invertible (for nonzero noise) because the determinant $D_1=1+u_n^2-2u_n\cos(2\pi n\Theta)\ge 1+u_n^2-2u_n=(1-u_n)^2>0$. Hence the Fourier coefficients of $p_1^*(\psi)$ are uniquely solvable as functions of a_n, b_n, c_n, and d_n.

For ϵ sufficiently small we may approximate the stochastic winding number as

$$\Omega_{A,\text{stoch}}=1+\frac{1}{T_B}\int_0^1 R(\theta)q^*(\theta)d\theta$$
$$\approx 1+\frac{1}{T_B}\int_0^1[a_0+\epsilon r(\theta)][1+\epsilon q_1^*(\theta)]d\theta$$
$$=1+a_0\omega_B+\frac{\epsilon^2}{T_B}\int_0^1 r(\theta)q_1^*(\theta)d\theta=1+a_0\omega_B$$
$$+\frac{\epsilon^2\omega_B}{2}\sum_{n=1}^{\infty}(a_n\ b_n)\begin{pmatrix}\alpha_n(a_n,b_n,c_n,d_n)\\ \beta_n(a_n,b_n,c_n,d_n)\end{pmatrix}. \tag{28}$$

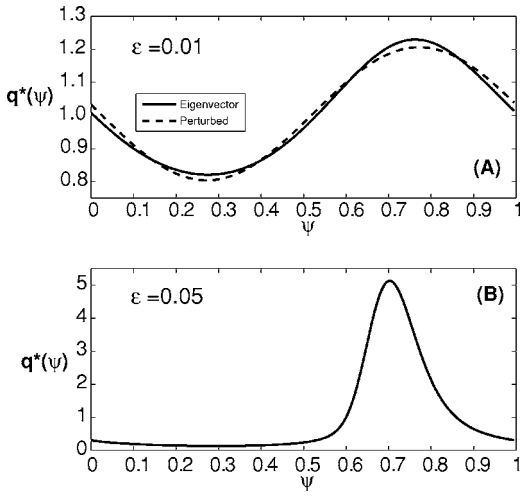

FIG. 3. (a) $q^*(\psi)$ calculated as the dominant eigenvector of G (solid line) and the perturbative solution (dashed line). Parameters are $f(\psi,\xi)=\psi+T_B+a_0+\epsilon\sin(2\pi\psi)+\xi$ with $T_B=1.25$, $\epsilon=0.01$, $\xi\sim N(0,\sigma)$, $\sigma=0.025$, and $a_0=-0.2$. (b) With the same parameters except $\epsilon=0.05$ $q^*(\psi)$ can only be calculated as the dominant eigenvector of G as the perturbative solution is not valid for ϵ this large.

This calculation determines the phase-locking regions for $\epsilon>0$ that are preserved with the inclusion of noise. We expect even a small amount of noise to obscure long-period $j:k$: phase locking regions (j or k large). However, short-period phase locking regions like 1:1, 1:2, or 2:1 are expected to endure. The perturbative solution (28) provides a way to analyze the mechanism by which phase locking regions are damped by noise. Note, in particular, that higher order modes (n large) are damped by the factor $u_n=\exp[-2(n\pi\sigma)^2]$ such that $\sqrt{\alpha_n^2+\beta_n^2}\propto n\exp[-2(n\pi\sigma)^2]$ [see Eq. (27)]. This expresses concisely that long-period $n:m$ phase locking is destroyed by noise. By long-period phase locking we mean large n where n inputs lead to n distinct phase relations that tend to produce a growth in the amplitude of the nth Fourier mode of $q_1^*(\psi)$. Figure 3 shows calculations of $q^*(\psi)$ for both the dominant eigenvector solution [solid line in panels (a) and (b)] and the perturbative solution [dashed line in panel (a)] for the sine circle map $f(\psi,z)=\psi+a_0+\epsilon\sin(2\pi\psi)+z$ for a stimulation frequency ($\omega_B=0.8$) in the 1:1 phase locking region. For $\epsilon=0.01$ the perturbative solution is in agreement with the eigenvector solution. If $\epsilon=0.05$ the perturbative solution is no longer valid as the eigenvector solution exhibits strong 1:1 statistical phase locking.

For ϵ sufficiently small and if $s(x)=0$, i.e., c_n and d_n are zero for all n, then the perturbative stochastic winding number is

$$\Omega_{A,\text{stoch}}\approx 1+a_0\omega_B-\frac{\epsilon^2\omega_B}{2}\sum_{n=1}^{\infty}\frac{2\pi n u_n(a_n^2+b_n^2)\sin(2\pi n\Theta)}{1+u_n^2-2u_n\cos(2\pi n\Theta)}. \tag{29}$$

Each term in the sum over n has a positive maximum and a negative minimum at the points

$$\Theta=\frac{k}{n}\pm\frac{1}{2\pi n}\cos^{-1}\left(\frac{2u_n}{1+u_n^2}\right),\quad k\in\mathbb{Z}, \tag{30}$$

respectively. Hence, increasing the input frequency $\omega_B=1/T_B$ so that $\Theta=T_B+a_0$ varies between these two points generates a monotonically increasing contribution to the stochastic winding number. Thus we can estimate the width of a paradoxical segment arising from the nth mode as $\Delta T_B=(1/\pi n)\cos^{-1}[2u_n/(1+u_n^2)]$. Recall that $u_n=\exp[-2(n\pi\sigma)^2]$. Hence, as σ is increased the width of the paradoxical segment is increased slightly, but not exceeding $1/\pi n$, but the amplitude diminishes proportionally to u_n. Furthermore, the nth order firing rate perturbation magnitude is proportional to $\epsilon^2(a_n^2+b_n^2)$. That is, if $r(x)$ does not contain the nth Fourier mode then no information regarding the corresponding paradoxical segments will be revealed by the first-order perturbative method. The solution does not exist in the small noise limit $\sigma\to 0$ because the linear system (27) becomes singular and the invariant density converges to the set of delta functions about the phased locked points ψ^* if in a phase locking region, or converges toward an ergodic measure on some quasiperiodic orbit that densely fills the circle. Thus the smoothness assumption breaks down in the phase locking regions and the invariant density cannot be expanded as a Fourier series. This also suggests that at the center of the paradoxical region the error between the perturbative solution and the analytical solution will be the greatest. Hence σ and ϵ must scale together for the perturbative solution to be valid. A larger ϵ makes for a larger deterministic phase locking region and hence σ must also be increased in order to obscure strong phase locking. The surprising result is that the first-order perturbative solution reveals that the $n:m$ quasi-phase-locking regions exist at the $O(\epsilon^1)$ level only if the phase resetting curve $r(\phi)$ contains nth order Fourier modes. For example, take the deterministic sine circle map $\phi\to\Theta+\phi+\epsilon\sin(2\pi\phi)$ which has $n:m$ phase locking regions centered about the points m/n on the Θ axis each with $O(\epsilon^n)$ width [20]. With the addition of noise the $n:m$ quasi-phase-locking regions with $n\geq 2$ may only persist at the $O(\epsilon^2)$ level and therefore have $O(\epsilon^3)$ magnitudes which are effectively nonexistent. The result also shows that, in the case of weak phase-dependent coupling (small ϵ), the $n:m$ paradoxical segments all possess the same mechanism by which noise diminishes their width and magnitude and that the modes are independent of one another, suggesting that the above sine circle map is a good candidate as a model system because the inclusion of higher Fourier modes is redundant, merely creating additional noninteracting phase locking regions on a finer scale.

C. Example: Noisy sine circle map

Using the above rationale we take the stochastic sine circle map $f(\phi,\xi)=\Theta+\phi+\epsilon\sin(2\pi\phi)+\xi$ as the canonical system. Figure 4 shows the stochastic winding number calculated from the full $q^*(\phi)$ (thick solid line) and the perturbatively calculated $q^*(\phi)$ (thick dashed line), both overlaid atop the numerically calculated deterministic winding number (thin dashed line) as in Eq. (16) for large n, over three

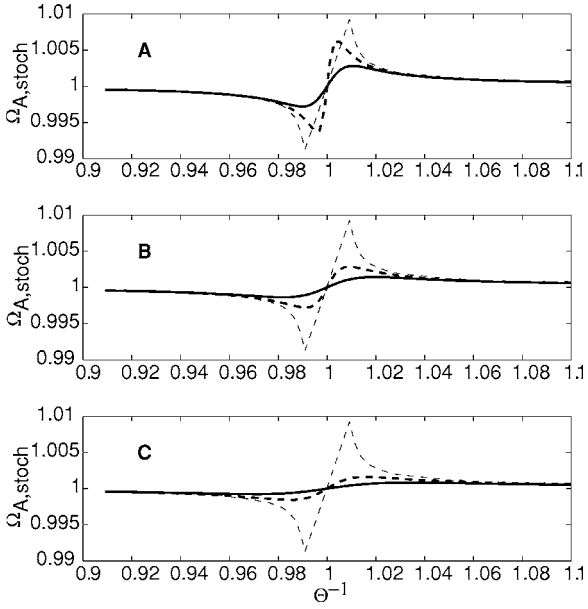

FIG. 4. Calculations of the stochastic winding number $\Omega_{A,\text{stoch}}$ for the sine circle map through a frequency sweep from $\Theta^{-1}=0.9$ to $\Theta^{-1}=1.1$ with model parameters $a_0=0$, $\epsilon=0.01$, and $\sigma=0.05$, 0.1, and 0.15 represented in panels (a), (b), and (c), respectively. The thick solid line is the actual stochastic winding number; the thick dashed line is the perturbative solution. For reference, the thin dashed line is the deterministic winding number that was numerically calculated as in Eq. (16) for large n. In all three plots 1:1 statistical phase locking produces the paradoxical region. Increased noise squashes the magnitude and broadens the width of the paradoxical region. Notice that the amplitude of the singularly perturbed solution is not a good match to the actual solution but the minima and maxima provide a good approximation to the size of the paradoxical region.

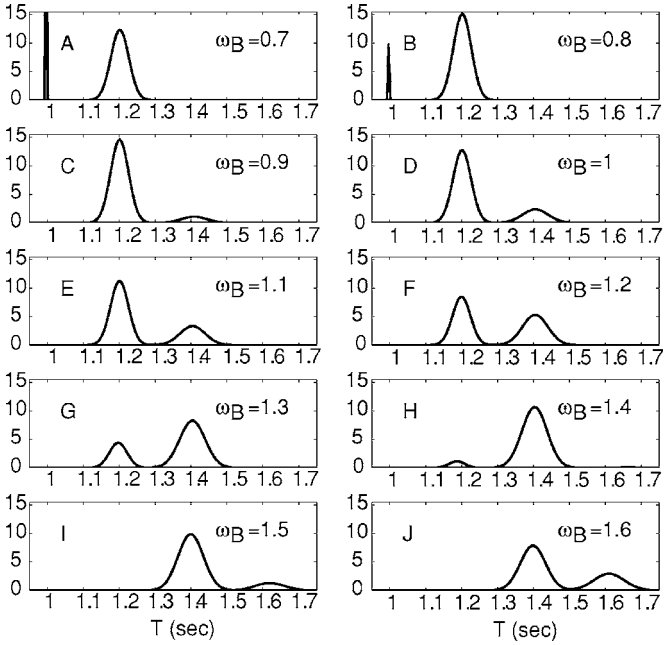

FIG. 5. Calculations of $p_{AA}(T)$ for the noisy circle map with no phase dependent coupling ($\epsilon=0$) through a frequency sweep from $\omega_B=0.7$ to $\omega_B=1.6$. Model parameters are $a_0=-0.2$ and $\sigma=0.025$.

different noise levels [panels (a), (b), and (c)]. The paradoxical region, due to 1:1 statistical phase locking, diminishes in magnitude with an increase in noise while the width of the minima and maxima gets slightly wider according to $\Delta\Theta^{-1}=\pi(\cos^{-1}[2u_1/(1+u_1^2)])^{-1}$. The perturbative solution provides an approximation to the width of the paradoxical region however for smaller noise levels [panel (a)] the vertical magnitude is not a good match because the $O(\epsilon^2)$ terms become relevant in the paradoxical region. Outside the paradoxical region however the errors become minuscule. Hence, in putative paradoxical region where statistical phase locking exists the perturbative solution provides a marker for the existence or nonexistence of the paradoxical regions and estimates of their size, but does not accurately approximate the true shape of the stochastic winding number. This suggests that higher order terms are necessary to elucidate exactly the shape of the paradoxical region.

The singularly perturbed solution shows the emergence of firing rate perturbations emerging from the zeroth order state $q^*(\psi)=1$, where no reliable phase relationships exist. If ϵ is made larger, the singularly perturbed solution is no longer valid but the phase locking regions become large enough to be physiologically relevant, and the effects of phase-dependent coupling will be readily seen in spike patterning of the ISI distribution. Figure 5 shows the ISI distribution for the sine circle map for when there is no phase-dependent coupling ($\epsilon=0$) for a frequency sweep $\omega_B=0.7$ to $\omega_B=2$, in 0.1 increments. Unlike the previous case shown in Fig. 4 we set $a_0=-0.2$. The spike patterning without any phase dependent coupling ($\epsilon=0$), when there is no statistical phase locking, serves as a comparison for the $\epsilon>0$ case. At $\omega_B=0.7$ [panel (a)] the input frequency is slower than the oscillator intrinsic frequency and the oscillator can be found in two distinct firing periods, one representing the cycles where no input was given, represented by a delta pulse centered about unity, and a bell-shaped density of periods centered about $T=1.2$ representing those that received a single input. As the input frequency is increased [panel (b)] the proportion of cycles not receiving input shrinks. At $\omega_B=0.9$ [panel (c)] the noninput cycles are gone and a bimodal distribution emerges where the larger left mode are cycles receiving a single input and the right mode are cycles receiving two inputs. As the input frequency increases further the left mode shrinks while the right mode grows [panels (d)–(h)]. At $\omega_B=1.5$ [panel (I)] there are no longer any cycles receiving only a single input and an additional mode emerges of cycles receiving three inputs. Note also that this ISI distribution bears resemblance to the ISI distribution for $\omega_B=0.9$ except that the two modes are slightly broader reflecting the increased uncertainty from receiving a greater number of stochastic inputs. In a similar fashion, this cycle repeats as the input frequency is increased further to $\omega_B=1.6$ [panel (j)] and beyond, where the ISI distribution probability mass moves rightward by the emergence and growth of modes centered about $T=1-ka_0$ for $k=0,1,2,\ldots$.

For the case of strong phase-dependent coupling we choose $\epsilon=0.1$, which is too large to use the singularly perturbed solution so we must solve for the fixed point of G (5)

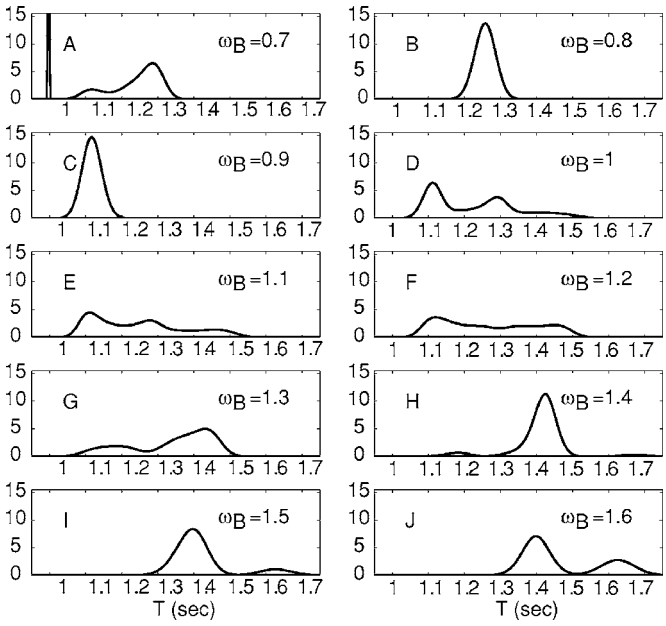

FIG. 6. Calculations of $p_{AA}(T)$ for the noisy circle map through a frequency sweep from $\omega_B=0.7$ to $\omega_B=1.6$. Model parameters are $a_0=-0.2$, $\sigma=0.025$, and $\epsilon=0.1$.

for $q^*(\psi)$. Figure 6 shows the ISI distributions for the same frequency sweep as before. The inclusion of phase-dependent coupling serves to radically shift the location of the probability mass compared to the $\epsilon=0$ case. The same general trend of the emergence of slower modes and shrinking of faster modes still holds as stimulation frequency is increased in the phase dependent case. At $\omega_B=0.7$ [panel (a)] the oscillator can be found at a wide range of periods. As the input frequency is increased [panel (b)] the ISI distribution narrows as the system enters the 1:1 phase locking regime. At $\omega_B=0.9$ [panel (c)] the 1:1 phase locking drives the entire population of cycles to shorter periods thereby producing the paradoxical region in the stochastic winding number plot (see Fig. 7). As the frequency is increased to $\omega_B=1$ [panel (d)] the system can no longer keep pace with statistical 1:1

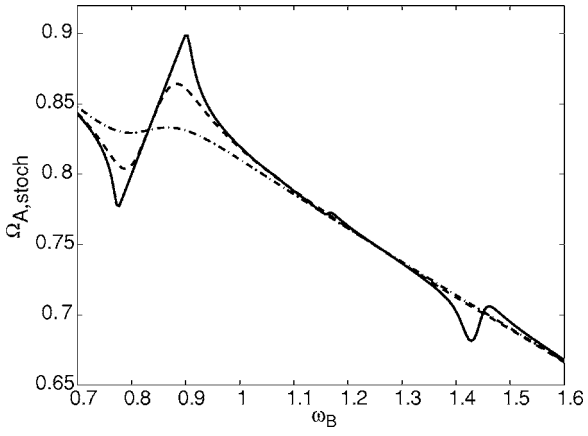

FIG. 7. Calculations of $\Omega_{A,\text{stoch}}$ for the noisy circle map through a frequency sweep from $\omega_B=0.7$ to $\omega_B=1.6$. Model parameters are $a_0=-0.2$ and $\epsilon=0.1$. Solid line represents $\sigma=0.025$, dashed line $\sigma=0.1$, and dot-dashed line $\sigma=0.2$

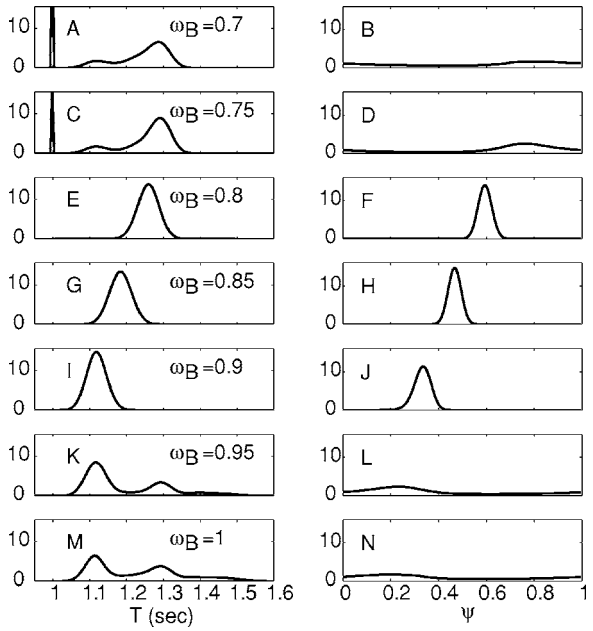

FIG. 8. Calculations of $p_{AA}(T)$ (left column) and the associated $q^*(\psi)$ (right column) for the low noise level ($\sigma=0.025$) sine circle map through a frequency sweep from $\omega_B=0.7$ through $\omega_B=1$. Model parameters are $a_0=-0.2$ and $\epsilon=0.1$.

phase locking every cycle and so the cycle periods shift radically to longer periods where the ISI distribution reveals a multi-modal shape. The leftmost mode are cycles still sustaining (1:1)-like firing rates while the right mode and the long rightward tail of the distribution represents cycles that have received two or more inputs before firing. Frequency increases beyond the quasi-(1:1) pattern [panels (e)–(g)] show the probability mass moving rightward to longer cycle periods while forming a very broad ISI distribution. At $\omega_B=1.4$ and beyond [panels (h)–(j)] the ISI distribution sharpens considerably about $T\sim 1.4$ forming a statistical 2:1 quasi-phase-locked pattern that evolves similarly to the non-phase-dependent case.

Figure 7 shows the stochastic winding number as a function of input frequency over three noise levels $\sigma=0.025$ (same level as in Fig. 6), 0.1, and 0.2 shown in solid line, dashed line, and dot-dashed line, respectively. The 1:1 paradoxical segment centered near 0.83 diminishes in amplitude with greater noise level. Note that for small noise $\sigma=0.025$ there exists a small 2:1 paradoxical segment and a very small 3:2 segment. Increased noise makes these regions barely detectable. In the weakly perturbed $O(\epsilon^1)$ solution these segments are not present suggesting that higher-order $O(\epsilon^2)$ processes are involved in larger n ($n=2, 3,\ldots$) quasi phase locking. Interestingly, if we included higher order Fourier modes in the phase response curve these paradoxical regions would scale in an $O(\epsilon^1)$ manner.

Furthering this analysis we show ISIs for a finer decrement of input frequencies near the 1:1 paradoxical region revealed in Fig. 7 alongside the associated distribution of invariant phases $q^*(\psi)$. Figure 8 shows the ISI distribution (left column) and $q^*(\psi)$ (right column) over a range of input frequencies in the 1:1 paradoxical region. The figure shows

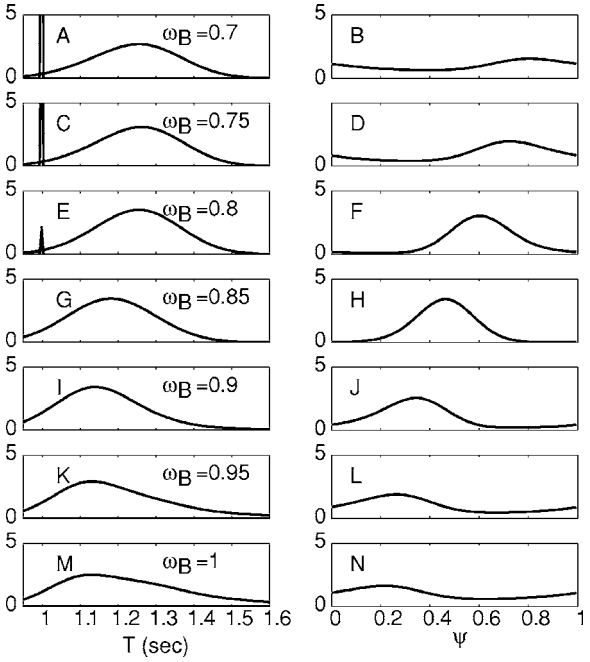

FIG. 9. Calculations of $p_{AA}(T)$ (left column) and the associated $q^*(\psi)$ (right column) for the higher noise level (σ=0.1) sine circle map through a frequency sweep from ω_B=0.7 through ω_B=1. Model parameters are a_0=−0.2 and ϵ=0.1.

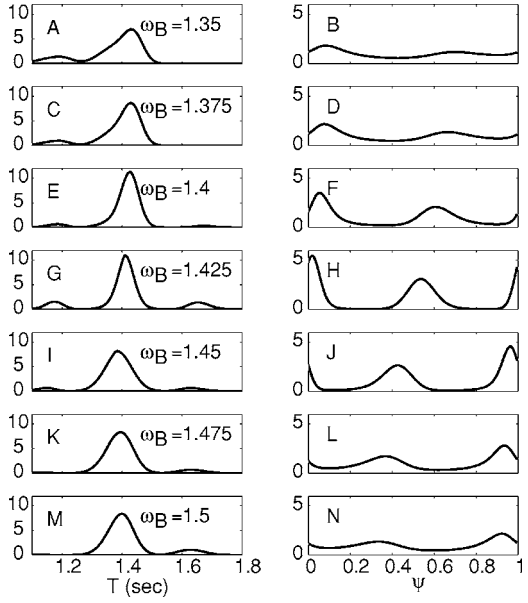

FIG. 10. Calculations of $p_{AA}(T)$ (left column) and the associated $q^*(\psi)$ (right column) for the low noise level (σ=0.025) sine circle map through a frequency sweep from ω_B=1.35 through ω_B=1.5. Model parameters are a_0=−0.2 and ϵ=0.1.

that the leftward shift of the ISI distribution to paradoxically faster cycles due to increased frequency is concomitant with the sharpening of the invariant phase density $q^*(\psi)$ to statistical phase locking.

The sharp structures in the firing patterns and phase densities seen in the low noise case are blurred substantially with an increase in noise. Figure 9 shows the ISI distributions and phase densities for the high noise (σ=0.1) for the same frequency sweep as in the low noise case. As previously, an increase in input frequency initiates a 1:1 quasi-phase-locked firing pattern thereby producing a sharpening of the phase density through the paradoxical region and first a leftward shift in ISI density followed by a larger rightward shift. In contrast to the low noise case, the sharpening of the phase density is not as great. In the high noise case the peaks of the ISI densities trace the leftward-rightward shifts very similarly to the low noise case. The real difference is that the rightward tail emerges sooner and is even longer than the low noise case and no bimodality emerges. This suggests that the mechanism of decreasing the size of the paradoxical region through increased noise is by decreasing the likelihood that the postsynaptic cell will be able to fire in time before the next input, which drastically slows the neuron.

In Fig. 7 a small 2:1 paradoxical segment exists near $\omega_B \sim 1.42$. To conclude this illustration we show in Fig. 10 the ISI distributions and $q^*(\psi)$ for a frequency sweep from ω_B =1.35 to ω_B=1.5, covering the 2:1 paradoxical segment shown in Fig. 7 under low noise conditions (σ=0.025). Over this sweep of frequencies the invariant phase density sharpens to form a bimodal distribution suggesting a 2:1 quasi-phase-locked state. In this case typically two inputs occur before the postsynaptic oscillator can fire.

IV. DISCUSSION

Using the stochastic phase model (3) we have shown how to analytically construct the relative timing of input distribution $p_{AB}(\tau)$ and the ISI distribution $p_{AA}(T)$. These analytic constructions are faster to compute than Monte Carlo simulations and have the advantage of being analyzable. Using the stochastic winding number [8], we compute the perturbative stochastic winding number for ϵ-small phase-dependent PRC and phase-dependent noise. Using these calculations we have explored the relationship between output firing rate in response to a sweep of inhibitory stimulation frequencies ω_B. In the absence of phase-dependent coupling (ϵ=0) there is no phase of the postsynaptic oscillator that is more likely to receive an input than any other ($q^*(\psi)$=1) and the stochastic winding number is independent of the noise level σ. With $0<\epsilon\ll 1$ paradoxical regions (regions of nonmonotonicity) in $\Omega_{A,\text{stoch}}(\omega_B)$ emerge and can be calculated as the inner product of $R(\theta)$ and the invariant distributions of phases $q^*(\psi)$. Increasing noise (σ) decreases the amplitude of paradoxical regions. Furthermore, by decomposing the $R(\theta)$ into its Fourier modes $n=1,2,\ldots$ we are able to show the $n:m$ paradoxical regions are functions of solely the nth Fourier mode. If the nth Fourier mode is small or nonexistent, then $n:m$ paradoxical regions will be small or not exist on an $O(\epsilon^1)$ level.

The spike patterning of a stochastic oscillator over a sweep of stimulation frequencies can be assessed by examining the ISI distribution. Under low-noise conditions, the characteristic shape of the ISI's is multimodal, where each mode represents a proportion of cycles receiving a certain number of inputs. Increased stimulation frequency causes a shift in probability mass away from modes of faster cycles and to modes of slower cycles. If the coupling is phase de-

pendent ($\epsilon > 0$), then $n:m$ paradoxical regions can exist and are a result of statistical phase locking, where the invariant distribution $q^*(\psi)$ narrows about m phase states that solve the fixed point equation for the deterministic map, for the case of $n:m$ phase locking. These statistical phase relationships serve to produce the characteristic left-then-right shift in probability mass due to increasing the stimulation frequency. The mechanism by which increased noise diminishes paradoxical left-then-right ISI density shifts due to $n:m$ statistical phase patterns is by increasing the likelihood that oscillators will either fire the mth spike before the nth input or, alternatively, be delayed too long and not be able to fire the mth spike before the $(n+1)$th input comes in. By increasing this likelihood, increased noise diminishes the sharpness of the multimodal peaks of the ISI distributions.

Using FP operators, in addition to producing the aforementioned statistical distributions, has the advantage of exploring the FP operator spectrum to find stochastic bifurcations [9,10,21–23]. Furthermore, in our examples, we have not examined the effects of a phase-dependent variance $S(\theta) \neq 1$. If S were to be larger in one section of the phase space relative to elsewhere it could disrupt phase locking preferentially in that section. Although those prospects are intriguing, we will defer their consideration for future work.

The techniques used in the current work could be extended beyond the present stimulation paradigm on a single neuronal oscillator to networks of coupled neural oscillators with noise. In some particular circle maps (see Ref. [24]) synchronization has been observed in coupled networks even in regimes of quasiperiodic flow or chaos. Synaptic noise, like that in the present work, could possibly disturb this synchronization of the network. In other neuronal models of all-to-all coupled networks of large $N \to \infty$ oscillators it is known that noise can serve to stabilize the incoherent state where the phase of one oscillator is not predictive of the phase of any other oscillator [25–27]. However, if N is of moderate size it is not known to what extent relative phase relationships or spike-timing relationships are important for the average firing rate of the constituent oscillators. This problem has relevance to light-intensity encoding by the marine invertebrate *Hermissenda* eye, whose five inhibitory photoreceptors encode light intensity via output firing rate. In this system, computational and physiological evidence suggests that noise disrupts photoreceptor phase locking, thereby obscuring paradoxical regions and permitting robust and systematic encoding [28,29]. The mathematical analyses presented herein indicate that this is a general phenomenon that extends beyond any particular system.

ACKNOWLEDGMENTS

W.H.N. is supported by NIMH R01-MH068392, RTG 0354259, and NSF DGE0217424. G.A.C. is supported by NIMH R01-MH068392. P.C.B. is supported by DMS 0515725.

[1] D. H. Perkel, J. H. Schulman, T. H. Bullock, G. P. Moore, and J. P. Segundo, Science **145**, 3627 (1964).
[2] J. P. Segundo, J. F. Vibert, M. Stiber, and S. Henneton, Neuroscience **68**, 657 (1995).
[3] J. P. Segundo, M. Stiber, J. F. Vibert, and S. Henneton, Neuroscience **68**, 693 (1995).
[4] A. F. Kohn, A. Freitas da Rocha, and J. P. Segundo, Biol. Cybern. **41**, 5 (1981).
[5] L. Glass and M. I. Mackey, *From Clocks to Chaos: The Rhythms of life* (Princeton Univ. Press. 1988).
[6] J. W. Fost and G. A. Clark, J. Comput. Neurosci. **3**, 137 (1996).
[7] M. Stiber, K. Pakdaman, J. F. Vibert, E. Boussard, J. P. Segundo, T. Nomura, S. Sato, and S. Doi, BioSystems **40**, 177 (1997).
[8] T. Yamanobe and K. Pakdaman, Biol. Cybern. **86**, 155 (2002).
[9] S. Doi, J. Inoue, and S. Kumagai, J. Stat. Phys. **90**, 1107 (1998).
[10] J. Inoue, S. Doi, and S. Kumagai, Phys. Rev. E **64**, 056219 (2001).
[11] A. D. Reys and E. E. Fetz, J. Neurophysiol. **69**, 1673 (1993).
[12] T. I. Netoff, C. D. Acker, J. C. Bettencourt, and J. A. White, J. Comput. Neurosci. **18**, 287 (2005).
[13] B. Ermentrout and D. Saunders, J. Comput. Neurosci. **20**, 179 (2006).
[14] C. Zhou and J. Kurths, Chaos **13**, 401 (2003).
[15] D. S. Goldobin and A. S. Pikovsky, Physica A **315**, 126 (2005).
[16] L. Glass, M. R. Guevara, J. Belair, and A. Shrier, Phys. Rev. A **29**, 1348 (1984).
[17] B. Ermentrout and N. Kopell, SIAM J. Appl. Math. **50**, 125 (1990).
[18] Y. Kuramoto, *Chemical Oscillations, Waves, and Turbulence* (Springer, 1984).
[19] A. Lasota and M. C. Mackey, Physica D **28**, 143 (1987).
[20] J. Guckenheimer and P. Holmes, *Nonlinear Oscillations, Dynamical Systems, and Bifurcations of Vector Field* (Springer, 2000), Vol. 42.
[21] B. Ermentrout and J. Rinzel, Am. J. Physiol. Regulatory Integrative Comp. Physiol. **246**, 102 (1984).
[22] R. Dodia, G. Svirskis, and J. Rinzel, J. Neurophysiol. **95**, 2664 (2006).
[23] T. Tateno, Phys. Rev. E **65**, 021901 (2002).
[24] G. V. Osipov and J. Kurths, Phys. Rev. E **65**, 016216 (1993).
[25] L. F. Abbott and C. van Vreeswijk, Phys. Rev. E **48**, 1483 (1993).
[26] W. Gerstner, Phys. Rev. E **51**, 738 (1995).
[27] N. Brunel and V. Hakim, Neural Comput. **11**, 1621 (1999).
[28] C. R. Butson and G. A. Clark, Abstr. Soc. Neurosci. **28**, 848.6 (2002).
[29] G. A. Clark, C. R. Butson, and W. H. Nesse, Abstr. Soc. Neurosci. **295**, 14 (2005).